A Demonstration of High Precision GPS Orbit Determination for Geodetic Applications

S. M. Lichten and J. S. Border
Tracking Systems and Applications Section

High precision orbit determination of Global Positioning System (GPS) satellites is a key requirement for GPS-based precise geodetic measurements and precise low-Earth orbiter tracking, which are currently being studied at the Jet Propulsion Laboratory (JPL). Different strategies for orbit determination have been explored at JPL with data from a 1985 GPS field experiment. The most successful strategy uses multi-day arcs for orbit determination and includes fine tuning of spacecraft solar pressure coefficients and station zenith tropospheric delays using the GPS data. Average rms orbit repeatability values for five of the GPS satellites are 1.0, 1.2, and 1.7 m in altitude, cross-track, and down-track components when two independent five-day fits are compared. Orbit predictions up to 24 hours outside the multi-day arcs agree within 4 m of independent solutions obtained with well-tracked satellites in the prediction interval. Baseline repeatability improves with multi-day as compared to single-day arc orbit solutions. When tropospheric delay fluctuations are modeled with process noise, significant additional improvement in baseline repeatability is achieved. For a 246 km baseline, with six-day arc solutions for GPS orbits, baseline repeatability is 2 parts in 10^8 (0.4–0.6 cm) for east, north, and length components and 8 parts in 10^8 for the vertical component. For 1314 and 1509 km baselines with the same orbits, baseline repeatability is 2 parts in 10^8 for the north components (2–3 cm) and 4 parts in 10^8 or better for east, length, and vertical components.

I. Introduction

The NAVSTAR Global Positioning System (GPS), when fully operational, will consist of a constellation of 18 satellites in 12-hour orbits designed to provide nearly continuous worldwide coverage for a variety of civil and military timing and positioning applications. For several years, the Jet Propulsion Laboratory (JPL) has been actively investigating GPS-based measurement systems with the goal of eventually demonstrating a sub-meter accuracy capability for GPS orbit determination. This capability will provide the basis for centimeter-level geodetic studies on a continental scale such as the NASA Geodynamics Program's Caribbean Initiative [1], [2] and decimeter-level positioning accuracy for low-Earth orbiters. A GPS-based measurement system will ultimately include GPS receivers situated at locations throughout the world to provide

accurate differential orbit determination for low-Earth orbiting satellites [3]–[5] such as TOPEX, the Earth Observing System, the Space Shuttle, and the Space Station, which will also be equipped with GPS receivers. Compared to other precise positioning systems such as very long baseline interferometry (VLBI), satellite laser ranging, and conventional ground tracking networks, GPS-based systems offer the potential for very high accuracy, an abundance of data, flexibility in the placement of ground receivers, and advantageous geometry provided by the high altitude and even distribution of the GPS satellites.

This article will discuss strategies for determining precise GPS orbits. Different aspects of orbit determination have been studied at JPL with 1985 experimental data processed through recently developed orbit and baseline estimation software. The 1985 GPS spring experiment took place between March 29 and April 5, 1985, representing the first of several GPS field tests conducted in 1985 and 1986. More than 20 institutions, including JPL, participated in the 1985 spring field test toward the goal of testing and evaluating GPS measurement techniques and equipment [1]. Data were acquired from seven developmental GPS satellites in orbit. TI-4100 GPS receivers [6] manufactured by Texas Instruments were placed at each of the ten ground sites in the continental United States. In addition, JPL SERIES-X receivers[1] were operated at the Mojave, California, and Owens Valley (OVRO), California, stations, and Air Force Geophysical Laboratory (AFGL) receivers, forerunners of the Macrometer II [7], were operated at the three POLARIS sites (Haystack, Massachusetts, Richmond, Florida, and Fort Davis, Texas). The POLARIS sites are collocated with VLBI radio telescopes used for geodetic and earth orientation studies. Water vapor radiometers (WVRs) were available at the Hat Creek, Mojave, and Owens Valley sites in California, while at other stations surface meteorological information was compiled during the experiment and used to correct the data for tropospheric delay. Table 1 and Fig. 1 summarize the experiment's configuration and the location of the ground receivers. Data were collected for about eight hours on each day of the experiment; however, because of the geometric constraints of the ground receiver configuration, GPS satellites were typically tracked for 2–4 hours before the receivers switched to new sets of satellites.

The GPS satellites transmit carrier signals at two L-band frequencies (1.22760 and 1.57542 GHz) which are modulated by a pseudo-random-noise code (P-code). All receivers in the field tests produce "carrier phase" observables from continuous tracking of the RF carriers. The TI-4100 receivers also produce a pseudorange observable by correlating the received modulated signal against a local copy of the code. The term pseudorange is used since this observable is a measure of the light travel time plus clock offsets at the satellite and the receiver. The carrier phase observable is analogous to "ambiguous range," since it measures range biased by an integer number of wavelengths. Both AFGL and SERIES-X receivers operate without knowledge of the P-code, although the SERIES-X receiver also generates a codeless pseudorange observable. Data from signals transmitted at the two frequencies are linearly combined to remove the dominant portion of the ionospheric delay, which varies inversely with the square of the frequency. Most of the results presented in this article are derived from the carrier phase data. Additional details on GPS signal structure and characteristics can be found in [8] and [9].

II. Data Processing

Data processing at JPL was conducted with the recently completed GIPSY (*G*PS *I*nferred *P*ositioning *SY*stem) software. GIPSY includes a comprehensive front end for data editing, phase connection, data compression, and atmospheric calibrations; PATH-VARY, a program which integrates the equations of motion and the variational equations to obtain nominal satellite trajectories and transition matrices for satellite states and dynamic model parameters; GPSOMC (*GPS O*bserved *M*inus *C*alculated), a module which calculates a very accurate model from best known nominal values and computes the pre-fit residuals and measurement partials; a U-D factorized batch sequential filter with process noise capabilities to perform parameter estimation and covariance analyses; and an output processor to display orbits, baselines, parameter solutions, and covariances. Clock modeling options include explicit single or double differencing, correlated process noise, and quadratic polynomials over specified data arcs. Additional details on specific modules in GIPSY can be found in [10].

Initially, GPS data processing, including parameter estimation, was performed separately for each day. Then multi-day arcs were formed, and longer runs were made covering up to six consecutive days. For some days, TI-4100 data were combined with the AFGL and SERIES-X data for orbit and baseline determination. However, since the different receiver types were in most cases collocated, there was not much to be gained (aside from an averaging effect on data noise) from processing all the data together—especially since with multi-day arcs, systematic effects as well as data noise become limiting error sources. Some of the TI-4100 data were used for determination of orbits and baselines independent of those based on the

[1] R. B. Crow, F. R. Bletzacker, R. J. Najarian, G. H. Purcell, J. I. Statman, and J. B. Thomas, "SERIES-X Final Engineering Report," JPL D-1476 (internal publication), Jet Propulsion Laboratory, Pasadena, California, 1984.

AFGL/SERIES-X network, and these separate solutions were compared to assess orbit and baseline repeatability.

III. Orbit Solution Strategy

The basic GPS orbit determination strategy includes simultaneous adjustment of the GPS orbits, station and satellite clock parameters, selected station locations, zenith tropospheric delays, range ambiguities (for carrier phase data), and solar pressure coefficients. There can be considerable variation in the way that these parameters are treated in the filter. In this section, various orbit determination strategies are described. In the next section, a comparison of orbit and baseline results using the different strategies is presented.

A. The Fiducial Concept

Fundamental to the GPS orbit determination performed at JPL is the fiducial network concept: a network of stations whose locations are accurately known from VLBI defines a self-consistent coordinate frame to which all GPS orbit and baseline solutions are referred. A detailed discussion of geophysical motivations for GPS geodesy, the selection of fiducial ground sites, and the validation of the fiducial concept with GPS measurements from the 1985 spring experiment can be found in [10]. Additional discussions of the role of GPS orbit determination in high precision geodesy can be found in [11] and [12]. An alternative to the fiducial approach, the free network approach, is discussed by Beutler *et al.* [13].

The results presented in this article are based on two basic fiducial network strategies. The first strategy has four fiducial ground stations, typically Haystack, Richmond, Fort Davis, and Owens Valley. This provides a well distributed set of reference points (Fig. 1). The second strategy has three fiducial points; the central Fort Davis station is adjusted along with the satellite orbits and other estimated parameters. Geometry provided by the second strategy is not as effective for defining the reference frame. However, in order to test baseline repeatability over long (>1000 km) distances, the second strategy was used for some of the solution sets. If Fort Davis or one of the other fiducial ground site locations were susceptible to systematic error or could be improved using the GPS data, the second strategy might be expected to produce better results.

B. Solar Radiation Pressure Model

The earliest GPS orbits determined at JPL showed that when fine tuning of the satellite solar pressure coefficients was not performed with simultaneous adjustment of station locations and GPS states, orbit and baseline repeatability was significantly degraded for data arcs longer than eight hours (single-day pass). If the solar radiation effects are left unmodeled, GPS position errors in down-track can increase to over 1 km after 1–2 weeks of integration of the equations of motion. Thus, even a small percentage error in one of the solar parameters can result in significant orbit errors. Solar radiation pressure is represented in the JPL software with the GPS Block I model [14], sometimes referred to as ROCK4. This model implicitly includes spacecraft component shapes, orientations, and masses and also accounts for inter-component shadowing. In ROCK4, it is assumed that the spacecraft remains perfectly oriented with respect to the sun. The spacecraft-centered coordinates defining the directions for solar radiation pressure accelerations (Fig. 2) have the Z-axis positive along the antenna directed toward the center of the Earth. The Y-axis is along the solar panel support beam, normal to the spacecraft–sun direction, and the X-axis is defined relative to the other two axes in the sense of a right-handed coordinate system. The force model represents the GPS spacecraft with 13 surfaces, each specified either as a flat surface or as a cylindrical surface. The flat surfaces are defined by length and width, while cylindrical surfaces are defined by radius of curvature, angle, and length. Each surface's reflectivity and specularity are represented by a number between 0 and 1 to account for varying absorption and diffusivity characteristics.

The solar radiation pressure results in a space vehicle acceleration

$$\ddot{\mathbf{r}} = P_1 \left[\frac{k^2}{\mathbf{r}_{ps}^2} (G_x a_x \hat{\epsilon}_x + G_z a_z \hat{\epsilon}_z) + G_y \hat{\epsilon}_y \right] \qquad (1)$$

where $\hat{\epsilon}_x$, $\hat{\epsilon}_y$, $\hat{\epsilon}_z$ are unit vectors for the spacecraft-centered coordinate system; the scalar P_1 is a shadow factor, 1 for direct sunlight, 0 for umbra, and between 0 and 1 for penumbra; $\mathbf{r}_{ps}$ is the spacecraft–sun vector; a_x and a_z are the space vehicle body fixed acceleration components determined by the ROCK4 model; k is the nominal Earth–sun distance (1 AU); G_x and G_z are solar pressure coefficient scaling factors; and G_y is a constant acceleration in the $\hat{\epsilon}_y$ direction, in km/sec^2, often referred to as the y-bias parameter.

The strategy adopted for fine tuning of the solar pressure parameters was to adjust G_x, G_y, G_z per satellite as constant parameters over the multi-day arc. Nominal solar radiation pressure parameters were taken from the precise post-fit ephemeris supplied by the Naval Surface Weapons Center (NSWC) [15]. The NSWC ephemeris was considered to be accurate in the WGS-72 reference frame to about 15–25 m (1 m in altitude and 15 m in each of the cross- and down-track components) and was determined from a two-week batch fit. The NSWC currently uses a more advanced software system known as the Multi-Satellite Filter/Smoother (MSF/S) [16] for generating reference GPS ephemerides. The *a priori*

uncertainties for the solar pressure coefficients for fitting at JPL from the March 1985 data were assumed to be 25 percent in x and z directions and 10^{-12} km/sec^2 for the y-bias. The NSWC fits in March and April 1985 vary from batch to batch typically by a few percent in the x and z coefficients and, for some satellites, by a significant fraction of 10^{-12} km/sec^2 for the y-bias. The JPL orbit strategy allowed somewhat more freedom in these solar pressure parameters in order to follow any shorter term variations which might be overlooked in the longer averaging period of the NSWC fits. In addition, the JPL orbits were determined with the x and z coefficients estimated as independent parameters. Nominally, these two parameters have the same value. This extra degree of freedom was left in the solution in order to absorb deficiencies in the solar pressure model and possibly to absorb other long term unmodeled accelerations. Some of the known limitations of the ROCK4 model, discussed by Fliegel *et al.* [17], could amount to orbit component errors of 4 m or more over a 14-day prediction interval. Allowing the JPL solar pressure parameters freedom to deviate from the nominal NSWC values was also motivated by the need to provide compensation for aliasing due to different parameter estimation strategies at JPL and NSWC. Finally, the geopotential model used in the NSWC fits (WGS-72 during March 1985) is slightly different from the GEM-L2 used in the JPL software. Because of these differences, NSWC and JPL force parameter solutions were expected to be slightly different.

The GPS x and z solar pressure parameter solutions obtained from a six-day arc covering March 31–April 5 were nearly all within 10 percent of the NSWC nominal values. The differences between the x and z coefficients were also generally less than 10 percent. The y-bias adjustments were somewhat larger, typically representing 25 percent changes from the nominal values. The adjustments for the GPS 6 solar pressure parameters were larger than those for the other satellites by a factor of about four. The reasons for this are not known, but these relatively large corrections persisted regardless of the manner in which the data were analyzed.

C. Clock Modeling Strategies

The GIPSY software used at JPL for GPS orbit determination offers a number of options for receiver and transmitter clock modeling. These options include clocks modeled as polynomials, explicit single and double differencing, and clock behavior modeled as process noise. Most of the results presented in this article have all clocks modeled as white noise; at each measurement time, the clocks are considered to be independent of their values at other times. The effect is very similar to clock elimination through double differencing [18], although the white noise treatment has the advantage of eliminating the introduction of correlations between measurements through explicit differencing.

D. Treatment of Tropospheric Delays

The troposphere is represented in GIPSY as a spherical shell which adds a delay to an incoming GPS signal:

$$\rho = \rho_{z_d} R_d(\theta) + \rho_{z_w} R_w(\theta) \tag{2}$$

where ρ_z is the tropospheric delay at zenith and R is an analytic mapping function developed by Lanyi [19] to map delays at zenith to the delay at elevation angle θ. The subscripts d and w refer to the dry and wet components of the tropospheric delay.

A priori values for zenith tropospheric delays were obtained from surface meteorology and, where available, from WVR measurements. The WVR measurements were converted to zenith delays using methods described by Robinson [20], and the surface meteorological measurements were converted to zenith delays using the Chao model [21].

The earliest GPS orbits determined at JPL relied on these *a priori* zenith delays for troposphere compensation. However, rms scatter was typically reduced by 50 percent or more when wet zenith delay corrections were estimated for each ground site in addition to the nominal calibrations. Various approaches to the troposphere estimation process were attempted, including not solving for tropospheric parameters at one or more WVR sites and varying the *a priori* uncertainty from 2 to 20 cm for the wet zenith delay parameter. For multi-day arcs, the zenith wet troposphere parameters were initially modeled with process noise in such a way that the troposphere values from one day to the next were independent but behaved as constants on any given day. Subsequently, in an effort to follow tropospheric fluctuations on time scales ranging from six minutes to several hours, the process noise time constraint was relaxed so that the tropospheric zenith delay could change slowly during the eight hour tracking period.

Two basic process noise models were used to model tropospheric fluctuations: colored noise and a random walk. The process noise formulation in the GIPSY filter is for first order exponentially correlated process noise, as described in detail by Bierman [22] and by Wu *et al.*[2] A brief summary of the formulation from those references is given here.

Let $p(t)$ be the value of a time-varying stochastic parameter and let $\omega(t)$ be a white process noise with zero mean value.

[2] S. C. Wu, W. I. Bertiger, J. S. Border, S. M. Lichten, R. F. Sunseri, B. G. Williams, P. J. Wolff, and J. T. Wu, "OASIS Mathematical Description," vol. 10, JPL D-3139 (internal publication), Jet Propulsion Laboratory, Pasadena, California, 1986.

The GIPSY filter and smoother are formulated in terms of discrete time intervals referred to as batches. At the end of the jth batch, the process noise parameters are updated:

$$p_{j+1} = m_j p_j + w_j \tag{3}$$

where $p_j = p(t_j)$ and $p_{j+1} = p(t_{j+1})$. The exponential multiplier, m_j, is defined as

$$m_j = \exp\left[-(t_{j+1} - t_j)/\tau\right] \tag{4}$$

where τ is the process noise time constant.

The discrete time-varying variance for a stochastic parameter is

$$\sigma^2_{p_{j+1}} = m_j^2 \sigma^2_{p_j} + q_{\text{dis}} \tag{5a}$$

$$= m_j^2 \sigma^2_{p_j} + (1 - m_j^2)\sigma^2_{ss} \tag{5b}$$

The steady-state sigma, σ_{ss}, is the noise level approached after the system has been operating undisturbed for a time much greater than τ. Together τ and σ_{ss} define the process noise variance in discrete form, q_{dis}.

The *random walk* is a special limiting case for Eq. (5). The random walk corresponds to $\tau \to \infty$. With a random walk, there is no steady state and σ_{ss} is not bounded, but q_{dis} is defined in the limiting sense

$$q_{\text{dis}} = \lim_{\tau \to \infty} \frac{\sigma^2_{ss}}{\tau} \tag{6}$$

Note that for a random walk, q_{dis} is related to the Allan variance $\sigma^2_A(\Delta t)$:

$$\sigma^2_A(\Delta t) = \frac{q_{\text{dis}}}{\Delta t} \tag{7}$$

Table 3 lists various process noise troposphere estimation strategies which were attempted in filtering the March 1985 GPS data. The second column of Table 3 shows the magnitude of the process noise for various models—either σ_{ss} for the correlated process noise cases or, for the random walk cases, the cumulative effect of q_{dis} [Eq. (6)] over one day.

IV. Orbit Determination Results

A. Coordinate Systems

Nominal orbits used to initialize the filter were supplied by the NSWC. In the spring of 1985, these orbits were computed in the WGS-72 coordinate system and were expected to be accurate to about 15–25 m. The fiducial stations used for the precise GPS orbit determination in this experiment are defined in the VLBI coordinate system, however, and thus a relatively large orbit adjustment was expected which would compensate for the difference (mostly a rotation in longitude) between the two coordinate systems. An accepted value for the coordinate rotation is 0.554 arc sec (2.6 μrad), although published values range from 0.5 to 0.8 arc sec [23]. A rotation of 0.554 arc sec corresponds (S. C. Wu *et al.*, see footnote 1) to approximately 15 m movement for a ground station and about 70 m at GPS altitude.

In order to empirically determine the coordinate system offset with the GPS data, a filter run was set up covering six days from March 31 to April 5. The only parameters estimated in this run were UT1–UTC, X and Y polar motion, and white process noise satellite and non-maser station clocks. Those station clocks which were using hydrogen masers as time standards were modeled in successive runs as linear and quadratic polynomials and as uncorrelated white process noise. The results were essentially independent of the clock model used for the masers. The solution for UT1–UTC was about 3.3 μrad, or approximately 0.68 arc sec. The X and Y polar motion solutions were at least an order of magnitude smaller. The difference between the JPL GPS result (0.68 arc sec) and the published value (0.554 arc sec) can be almost totally explained by the difference between the nominal earth orientation values supplied by the International Radio Interferometric Surveying Subcommission (IRIS) and those supplied by the Defense Mapping Agency (DMA). The IRIS values are used in GIPSY, while the DMA values were used by the NSWC for GPS orbit fitting. The difference between the DMA and IRIS UT1–UTC values for March 25, 1985, is 0.13 arc sec, which, when combined with the 0.554 arc sec assumed value for the WGS-72 to VLBI coordinate system rotation, is very close to the 0.68 arc sec determined for the JPL GPS solution.

Figure 3 shows two orbit fits for GPS 8 (we use the Navstar number to identify the satellites) from the six-day arc. Table 2 describes the basic orbit determination strategy used for these and most subsequent GPS solutions. Nearly all adjusted parameters were estimated with very large *a priori* uncertainties. The

data weights used for all solutions in this article were greater than the carrier phase intrinsic receiver noise of several millimeters in order to be consistent with post-fit rms scatter and in order to make $\chi^2_\nu \simeq 1$, where

$$\chi^2_\nu = \frac{\sum_{i=1}^{n} \left(\frac{z_i(\text{obs}) - z_i(\text{pred})}{\sigma_i} \right)^2}{n - m} \qquad (8)$$

In this expression, n and m are the number of measurements and degrees of freedom, z_i(obs) and z_i(pred) are the observed range and predicted post-fit range for the ith measurement, and σ_i is the measurement noise for the ith measurement. The data weights used were based on this criterion and correspond to measurement noise of about 0.9–1.5 cm, depending on the length of the data arc.

The solution plotted in Fig. 3(a) includes the coordinate system offset discussed above; most of the rotation shows up in the cross- and down-track orbit components. Figure 3(b) shows a solution from a filter run identical to the first except that a ~3 μrad coordinate rotation in UT1–UTC (longitude) was first included in the model before estimation of parameters. The large cross-track amplitude has been greatly reduced, since it is mostly due to the rotation of coordinate systems. The down-track run-off can be attributed to a slight overall altitude correction to the satellite ephemeris; because the orbital period changes with altitude, the down-track correction will slowly increase over time. An overall altitude adjustment of 70 cm, for example, would cause a run-off in the down-track component of about 7 m per orbit, roughly what is observed in Fig. 3(b). The NSWC nominal orbits are expected to be accurate to about 1 meter for the altitude component alone, so the results plotted in Fig. 3 are consistent.

B. Orbit Precision and Accuracy

Since the effective measurement noise was increased to be consistent with the post-fit rms scatter, the formal errors from the filter are one measure of the precision of the orbits. Figure 4 shows plots of formal orbit errors from a six-day arc solution and a single-day arc solution for GPS 8 and GPS 6 fit with carrier phase. GPS 8 was well tracked throughout the experiment, while GPS 6 was more sparsely tracked, with good geometry lasting only a few hours each day. The oscillatory nature of the error magnitude is due to tracking limitations, since the satellites were observed only from the continental United States each day. The single-day run included data from nine tracking sites, whereas the six-day run had only five to partially compensate for the greater quantity of data in the long arc. Figure 4 indicates that orbit precision of about 0.2–1.5 m is to be expected from multi-day arcs for well-tracked satellites, and about 0.5–3.0 m is to be expected for more sparsely tracked satellites. For one eight-hour pass (single-day arc), the formal errors are somewhat higher—1–3 m for GPS 8 and 2–8 m for GPS 6.

It is important to distinguish between orbit precision and accuracy. The formal orbit errors will in general underestimate orbit accuracy as a result of systematic effects which do not appear in post-fit scatter or which cannot be well compensated for simply by raising the effective measurement noise. A number of systematic errors which could grow slowly over time might not be apparent from post-fit scatter; such systematic effects could result from mismodeling of the earth's geopotential, from long-term spacecraft accelerations due to mismodeled solar radiation pressure or other unmodeled forces, or from earth orientation errors and fiducial station coordinate errors. Thus, comparisons between solutions derived from data sets in which different receivers and/or different data arcs were used may provide a better measure of orbit accuracy than would formal errors.

In order to better assess GPS orbit precision and accuracy, a set of single- and multi-day arcs was set up as shown in Fig. 5. Arcs A and B cover three days each and do not overlap in time. Arcs C and D cover five days each and do not have any data in common, although they overlap in time. Data on March 30 were also used to obtain GPS orbits completely independently of solutions obtained with the six-day arc covering March 31–April 5. These different sets of orbits were compared to measure orbit repeatability. In all the comparisons involving multi-day arcs, the solutions were compared over a "neutral" time interval outside the periods during which data were taken, so these comparisons provide a rather stringent test of the robustness of the orbits and models used to propagate and predict up to 24 hours outside the data arcs.

Figure 6(a) summarizes the GPS orbit repeatability for arcs A and B. These results show repeatability based on solutions in which the zenith troposphere at each site is adjusted as a constant bias independent from one day to the next. The overall average unweighted rms differences are 1.2, 2.9, and 2.6 m in altitude, cross-track, and down-track components for five satellites, averaged over a six hour period whose midpoint was about eight hours away from the nearest measurements. Figure 6(b) shows the corresponding GPS orbit repeatability for arcs C and D with constant zenith tropospheric delay parameters estimated. The overall average rms differences are reduced to 1.1, 1.5, and 2.4 m in altitude, cross-track, and down-track components. Figure 6(c) shows repeatability for arcs C and D with tropospheric zenith delay modeled with process noise as a random walk (first entry in Table 3). A noticeable improvement is apparent when Fig. 6(c) is compared to parts (a) and (b). With the process noise troposphere strategy, the average rms differences are further reduced to 1.0, 1.2, and 1.7 m in altitude, cross-track, and down-track components. Figure 7

shows sample orbit comparisons for GPS 8 and GPS 6 corresponding to the stochastic troposphere strategy of Fig. 6(c).

Figures 6 and 7 make a strong case for fine tuning the tropospheric delay parameters using process noise. Other troposphere process noise models showed similar improvement over the constant troposphere method, but the random walk model for tropospheric delay fluctuations gave the best orbit repeatability. Table 3 lists some of the troposphere strategies used and notes those which worked best as judged by orbit and baseline repeatability. Treuhaft and Lanyi [24] have developed a model for tropospheric delay fluctuations which behaves in a manner similar to a random walk over time scales of several minutes or longer and shows agreement with VLBI data. For shorter time scales, the Treuhaft and Lanyi model has characteristics of both a Markov process and a random walk. However, the tropospheric parameters estimated from the GPS data are residual delays due to limitations of the calibrations (from surface meteorology or WVRs) whose behavior is not easily modeled. We proceeded on the assumption that residual tropospheric delays after calibration behave in a manner similar to the tropospheric fluctuations themselves, although presumably with reduced amplitudes. All of the rms differences shown in Figs. 6 and 7 are consistent with the formal errors (1-σ) from the orbit fits. Figures 6 and 7 also seem to indicate that with essentially similar data and geometry, a five-day arc is preferable to a three-day arc for GPS orbit determination. However, it should also be noted that arcs A and B have no temporal overlap whatsoever; their repeatability is based on orbit prediction of up to 12 hours outside the data arcs and should be somewhat more sensitive to systematic errors which grow with time. The C-D repeatability, however, is based on interpolated orbits at times between five and eleven hours from measurements but still within the interleaved data arcs.

Figure 8 shows orbit repeatability using single day arcs. A single day typically included 6–7 hours of GPS data; GPS 8 was tracked for the entire data collection period, while the other spacecraft were tracked for periods ranging from one hour to four hours. Therefore, in contrast to the multi-day arcs, the amount of data and the geometry are very limited in a single day arc. The day shown in Fig. 8 is March 30. As typically happens during experiments of this kind, there were various equipment difficulties on March 30, including considerable data loss from the northeast which compromised viewing geometry. Although March 30 was not the worst day in terms of technical problems, for this experiment its data were definitely below average in quality as a consequence of data loss.

Figure 8(a) compares orbits from March 30 data for GPS 8 in which one orbit solution is from TI receivers and the other is from SERIES-X and AFGL receivers. Because one of the SERIES-X receivers (Owens Valley) was inoperative on March 30, the non-TI data set includes data from only four stations. Because of the data loss, the formal errors were relatively large when station clocks were modeled as white process noise. However, when the stations with maser time standards had their clocks modeled as polynomials, the formal errors decreased to a sufficient degree to make the comparison meaningful. The AFGL receivers at Richmond and Fort Davis and the SERIES-X receiver at Mojave were running on hydrogen maser clocks. The Haystack TI receiver used a crystal oscillator. The crystal clock fluctuations could be modeled as white process noise but not as a linear or quadratic polynomial. Figure 8(a) shows agreement at the 1 m level between the TI and non-TI orbits for March 30. It is instructive to see that even with a compromised data set, the stability of some of the station clock standards permitted clock modeling which improved the orbit for this satellite. Figure 8(b) compares the March 30 GPS 8 orbit with the GPS 8 orbit predicted back a full day from the six-day arc covering March 31–April 5; the orbits still agree at the 3 m level.

Figure 9 shows orbit repeatability with a one-day versus a multi-day arc for GPS 6, a satellite representative of those with somewhat sparse ground coverage. The single-day/multi-day comparison is not as good as with GPS 8, a well-tracked satellite (see Fig. 8). However, the multi-day/multi-day comparisons for GPS 6 match–and, for some components, even slightly surpass–repeatability for GPS 8 (see Figs. 6 and 7). Thus, without use of *a priori* knowledge of satellite trajectories, 1–2 m orbit repeatability is possible for both well tracked and sparsely tracked satellites with multi-day arcs, but only well-tracked satellites can achieve this level of repeatability with a single pass on one day for the limited configurations of this experiment. This is also reflected in the formal errors, which for sparsely tracked GPS were 5–10 m for the single day arc but decreased to 1–3 m with the multi-day arcs.

C. Baseline Repeatability

Baseline repeatability is often used to assess orbit quality in a geodetic context. Baseline repeatability tests have the advantage of not requiring any orbit propagation or prediction. A six-day arc was arranged to test baseline repeatability. Five ground receivers (Haystack, Richmond, Fort Davis, Mojave, and Owens Valley) were used in these solutions, with Fort Davis and Mojave station locations estimated each day independently. For each day of the multi-day arc, these station positions were reset with a large *a priori* uncertainty and were estimated anew with the data from that day. One set of smoothed orbits was generated based on all the data, including data from the two estimated stations. The rms scatters about the weighted means of the components of the Mojave–OVRO, Mojave–Fort Davis, and Fort Davis–OVRO baselines (246, 1314, and 1509 km) were calculated.

The baseline repeatability results are shown in Fig. 10. Figure 10(a) shows the Mojave–OVRO baseline, including a comparison of three different orbit estimation strategies: single-day pass solutions, multi-day arc solutions, and multi-day arcs with troposphere modeled as process noise. The multi-day arc solutions are more consistent than the single-day solutions for the 246 km baseline. The stochastic troposphere modeling strategy dramatically improves the 246 km baseline repeatability further; all components are consistent at the 0.5 cm level except for the vertical (2.0 cm). Parts (b) and (c), which give results for the longer baselines, show less dramatic improvement in all components than that seen in part (a) for the 246 km baseline with the troposphere process noise strategy. However, the components showing highest rms scatter still show moderate improvement. For the shorter baselines, it appears that fluctuating tropospheric delay can be a dominant systematic error source affecting repeatability if left unmodeled, but for the continental baselines, orbit errors and fiducial network errors may be more important. All baseline components over 246–1509 km show repeatability of 2–4 parts in 10^8 except for the vertical component for Mojave–OVRO (eight parts in 10^8).

It was noticed that Mojave–OVRO repeatability showed a slight but significant improvement when the Fort Davis position was adjusted as compared to solutions when Fort Davis was fixed as a fiducial station. This should not happen if all the fiducial station positions are known *a priori* to within a few centimeters. Therefore, it is possible that both the orbits and the baselines being estimated are affected by as yet undetermined errors in the Fort Davis or other fiducial reference site locations. In general, Fort Davis (either the TI receiver or the AFGL receiver) was not adjusted because its position was considered well determined from VLBI techniques and because it is geometrically advantageous to have a fixed reference station centrally located in the United States. For the baseline repeatability tests, however, Fort Davis was adjusted in order to provide a long (more than 1500 km) baseline result. The GPS data should be capable of isolating and improving the station(s) with errors in nominal receiver coordinates. When this is done, in the future it is likely that accuracy for both orbits and baselines will further improve.

D. Use of the Pseudorange

Previous covariance analyses [25] have indicated that either pseudorange with measurement noise of 10–20 cm (for five minute averaging periods) or carrier phase with measurement noise of about 1 cm should be capable of providing orbit accuracy of 2–3 m with eight hours of data. In the spring 1985 GPS experiment, the carrier phase noise for six minute measurement averages was consistently below 1 cm, and when used to determine GPS orbits, those orbits have repeatability values slightly better than the 2–3 m predicted from the covariance analysis. However, the pseudorange data scatter was found to be larger than the expected 20 cm. Figure 11 shows carrier phase and pseudorange rms post-fit scatter from a solution in which pseudorange and carrier phase were processed together. The carrier phase post-fit rms scatter was uniformly between 0.5 and 0.6 cm for nearly all the receivers; however, the pseudorange rms was much larger than expected and was highly variable, ranging from 68 cm to as high as 225 cm. Ground multipath has been identified as a likely source of much of the pseudorange scatter [26]. Satellite multipath may also have affected the data, but with an amplitude of less than 15 cm [27].

Tests at JPL showed that a significant fraction of the pseudorange scatter could be removed by subtracting a multipath signature from the data; the multipath signature was determined by isolating the signal patterns which repeat from one day to the next. Nevertheless, the residual scatter was still too large for the pseudorange to be useful in a high precision orbit and geodetic context. GPS orbits from a single-day pass of pseudorange had formal errors (as well as repeatability) of about 20–30 m, much higher than the 1–4 m (1–2 m for multi-day arcs) levels obtained with carrier phase.

Despite the high pseudorange data scatter, a limited demonstration was performed to show the potential benefit of pseudorange. With a one-day pass on March 30, the TI-4100 pseudorange and the carrier phase data were processed simultaneously. Each data type was weighted according to its rms scatter, so nearly all the solution strength came from the high quality carrier phase data. Orbit repeatability was measured by comparing these combined data type March 30 orbits with the carrier-phase-only orbits from a five-station, six-day arc covering March 31–April 5. For satellites with even moderately good coverage, only a slight improvement (if any) in orbit repeatability was seen with the March 30 combined data type orbits compared to March 30 orbits from carrier phase only. However, several of the satellites on March 30 had very short tracking periods and limited geometric coverage, adverse factors which were further exacerbated by data loss which occurred for that day. With only carrier phase from a single-day pass, these weakly tracked satellites had rather large (5–10 m) formal orbit errors. Single-day March 30 orbits for these satellites showed significant improvement when pseudorange data was added to the carrier phase measurements, despite the high scatter of the pseudorange data. Figure 12 shows the improvement for GPS 3. Note that the improvement is significant for the cross-track and down-track components; these components are believed to be weakest with carrier phase because of the necessity of solving for range ambiguity parameters, which relate the observed range change from carrier phase to the transmitter–receiver absolute range. This

weakness in cross-track and down-track is related to a weakness in baseline solutions for eastern components often seen in carrier-phase-only solutions.

A covariance analysis was performed to evaluate the potential of combining high quality pseudorange with carrier phase for orbit and baseline determination. The geometry of the 1985 spring experiment was used for this simulation, with seven ground stations, including three fiducial stations. Figure 13(a) shows how progressively better pseudorange can improve orbits when combined with carrier phase data, particularly in the cross-track and down-track components. Adding high quality pseudorange to the precise (but ambiguous) carrier phase has an effect similar to that of bias fixing [18], [28], [29], since the pseudorange provides an absolute range measurement which can effectively constrain the carrier phase ambiguity. Figure 13(b) shows that the east component of a baseline improves considerably with the addition of pseudorange to carrier phase data if the pseudorange measurement noise is less than 50 cm. As a point of comparison, parts (a) and (b) also show predicted orbit and baseline errors for carrier range, which is carrier phase data for which all range ambiguities have been resolved. Note that the mixed data types provide accuracies approaching that which would be attainable if carrier range were available. With a single eight-hour pass, the predicted orbit errors are at the 1 m level or better, and the east component of the baseline is determined to about 3 parts in 10^8. Since the 1985 spring experiment had a limited configuration of ground receivers and satellites, it is expected that performance will improve further when the full GPS constellation is available. Figure 13 includes an error contribution from *considered* parameters based on a 4 cm assumed uncertainty in each component of the fiducial station positions. The errors from considered parameters are based on the sensitivity of the orbits or baselines to unadjusted parameters; these sensitivities are calculated from the measurement partials and geometry [22].

If steps are taken in the future to reduce multipath (e.g., through antenna design and placement and through use of ground plane absorbers), the combined pseudorange and carrier phase data types could become a powerful tool in high precision orbit determination and geodetic studies. The accuracies which would be possible with carrier range could be approached with combinations of carrier phase and sufficiently precise pseudorange.

V. An Orbit Error Budget for GPS

Formal orbit errors (Fig. 4) are based on the assigned data weights and on the *a priori* covariance for the estimated parameters. Since all the estimated parameters (except perhaps the tropospheric zenith delays) were basically unconstrained initially in the solutions, the data weights essentially determine what the formal orbit errors are. The data weights were set to be equal to the measurement noise scaled by a factor in accordance with Eq. (8) so that the weights were consistent with the post-fit scatter and with the number of measurements and estimated parameters. Typically, this scaling factor was between 1.0 and 1.5, which indicates that some residual systematic errors could be affecting the orbit solutions.

A consider covariance analysis was performed to examine the sensitivity of the orbit solutions to unadjusted parameters and to various potential systematic errors. As discussed above, the errors from considered parameters are combined with the formal errors computed in the filter to produce a total error covariance which includes the effects of likely systematic error sources whose effects are not compensated for in the basic solution strategy. Models for these unestimated parameters are used to calculate their effect on the orbits. Systematic errors included in this consider analysis were fiducial station location errors, errors in Earth orientation parameters, and uncertainty in the location of the Earth's geocenter relative to the fiducial stations. The consider analysis covered a six-day arc with five ground stations, including fiducials at Owens Valley, Richmond, and Haystack. Table 4 describes the assumptions for the analysis. The uncertainties in the earth orientation parameters specifying UT1-UTC and X and Y polar motion are based on the results of Spieth *et al.* [30] and Steppe *et al.* [31]. These uncertainties apply to earth orientation parameters which might be available several weeks after a GPS experiment; for real-time applications, uncertainties in the earth orientation parameters would be expected to be several times higher. Figure 14 shows the orbit error breakdown for GPS 8. Note that the expected root-sum-square (RSS) orbit errors are close to the 1–2 m orbit repeatabilities observed with multi-day arc (Fig. 6[c]). The two largest error categories are the computed (formal) error and the systematic errors from uncertainties in the fiducial station locations.

The computed error could be reduced by taking more measurements, lengthening the arc, including *a priori* information, or adding pseudorange. The number of measurements could be increased by the addition of more ground receivers, but as more GPS satellites are launched in the future, the amount of data will increase naturally. More *a priori* information could be included by using satellite and station clock models, WVR tropospheric calibrations at more sites, and better nominal orbits. Perhaps the most dramatic decrease in the computed error could be achieved if bias fixing were possible over long baselines [29]. With bias fixing, the east baseline component (corresponding to cross- and down-track orbit components) computed errors would decrease by at least a

factor of two. Even without bias fixing, the addition of pseudorange would similarly reduce the computed error, since it tightly constrains the carrier phase ambiguity parameters. With some types of receivers, pseudorange is available in addition to the carrier phase, but multipath must be reduced considerably before it is of sufficient quality to obtain sub-meter orbits in one pass. Lengthening the data arc beyond six days is feasible, but it might be more costly than some of these other remedies and might increase sensitivity to systematic errors from unmodeled accelerations.

Even if the computed contribution were reduced by a factor of two, the RSS orbit errors would still be over 1 m in cross-track and down-track if fiducial station position errors are 4 cm. Improvement in the fiducial station network requires painstaking refinement in the ties between the geodetic monuments and the GPS and VLBI antennas. Because it appears to be one of the limiting error sources, fiducial station accuracy is an area of intensive study at JPL.

The remaining systematic error sources in Fig. 14 are the earth orientation parameters (UT1–UTC, X and Y polar motion) and the location of the geocenter. These contribute relatively little to the total orbit error under the assumptions of the consider analysis but could become significant in the future as sub-meter GPS accuracy is approached. Note that although the earth orientation errors have a small but noticeable contribution to the GPS orbit error budget, the effect of these errors on differential measurements such as baselines is insignificant compared to other error sources [10]. The UT1–UTC error contribution in Fig. 14 applies only to the inertial reference frame (J2000); in an earth-fixed frame, the UT1–UTC error is eliminated in the transformation as long as the same value used in the orbit solutions is used to rotate to the earth-fixed frame. Most geodetic GPS applications, such as baseline determination, are based in an earth-fixed reference frame; thus, the UT1–UTC error would have essentially no effect, although it would introduce a bias in the GPS orbits.

Other systematic orbit errors result from unmodeled forces and accelerations which can affect the spacecraft trajectories. This category of errors includes spacecraft accelerations due to gravity mismodeling, gas leaks, solar radiation pressure mismodeling, and atmospheric drag. We believe that unmodeled accelerations of this type are small for GPS compared to other systematic effects, at least for arcs of one to several days. Preliminary consider analysis [25] shows very small perturbations (less than 5 cm down-track errors) from gravity field mismodeling for GPS orbits determined from carrier phase. In a future study, the analysis of gravity errors will be extended to cover longer arcs and to include the gravity field covariance matrix to model errors in the gravity coefficients. Since three solar radiation pressure coefficients were estimated for each satellite, we believe that our model has sufficient freedom to compensate for the solar radiation pressure forces as well as for some other minor spacecraft accelerations. When longer data arcs are available, these effects will be studied in more detail. Finally, the covariance studies found atmospheric drag at GPS altitudes to be insignificant, at least for data arcs of up to several weeks.

VI. Summary and Conclusions

Data from the spring 1985 GPS field test have been processed, and precise GPS orbits have been determined. With carrier phase data spanning five days, orbit repeatability is 1–2 m for each component, averaged for five satellites over a six hour period during which no data were taken. Baseline repeatability over the one-week period for a baseline of 246 km is about 2 parts in 10^8 (0.4–0.6 cm) for east, north, and length components; vertical repeatability is several times worse (8 parts in 10^8) for this baseline. Repeatability for two baselines of 1314 and 1509 km is 2–4 parts in 10^8 (3–5 cm) for all components.

Several refinements to the orbit determination strategies were found to be crucial to achieving these levels of repeatability and accuracy. These include fine tuning the GPS solar radiation coefficients and ground station zenith tropospheric delays. The time-varying behavior of the troposphere was modeled with process noise for the best results. Multi-day arcs of three to six days provided better orbits and baselines than the eight-hour arcs from single-day passes. A limited demonstration was able to show the potential for further orbit and baseline accuracy improvement with combined pseudorange and carrier phase data.

References

[1] J. M. Davidson, C. L. Thornton, C. J. Vegos, L. E. Young, and T. P. Yunck, "The March 1985 Demonstration of the Fiducial Network Concept for GPS Geodesy: A Preliminary Report," in *Proceedings of the First International Symposium on Precise Positioning with the GPS*, pp. 603–611, 1985.

[2] T. H. Dixon, M. P. Golombek, and C. L. Thornton, "Constraints on Pacific Plate Kinematics and Dynamics with Global Positioning System Measurements," *IEEE Transactions on Geoscience and Remote Sensing*, vol. GE-23, pp. 491–501, July 1985.

[3] T. P. Yunck, W. G. Melbourne, and C. L. Thornton, "GPS-Based Satellite Tracking System for Precise Positioning," *IEEE Transactions on Geoscience and Remote Sensing*, vol. GE-23, pp. 450–457, 1985.

[4] T. P. Yunck, S. C. Wu, and S. M. Lichten, "A GPS Measurement System for Precise Satellite Tracking and Geodesy," *J. Astronautical Sci.*, vol. 33, pp. 367–380, 1985.

[5] S. M. Lichten, S. C. Wu, J. T. Wu, and T. P. Yunck, "Precise Positioning Capabilities for TOPEX Using Differential GPS," *AAS Paper 85-401*, AAS/AIAA Astrodynamics Specialist Conference, Vail, Colorado, August 1985.

[6] D. J. Henson, E. A. Collier, and K. R. Schneider, "Geodetic Applications of the Texas Instruments TI 4100 GPS Navigator," in *Proceedings of the First International Symposium on Precise Positioning with the GPS*, pp. 191–200, 1985.

[7] J. W. Ladd and C. C. Counselman III, "The Macrometer II Dual-Band Interferometric Surveyor," in *Proceedings of the First International Symposium on Precise Positioning with the GPS*, pp. 175–180, 1985.

[8] R. J. Milliken and C. J. Zoller, "Principle of Operation of NAVSTAR and System Characteristics," *Navigation*, vol. 25, pp. 95–106, 1978.

[9] E. H. Martin, "GPS User Equipment Error Models," *Navigation*, vol. 25, pp. 201–210, 1978.

[10] J. M. Davidson, C. L. Thornton, S. A. Stephens, G. Blewitt, S. M. Lichten, O. J. Sovers, P. M. Kroger, L. L. Skrumeda, J. S. Border, R. E. Neilan, C. J. Vegos, B. G. Williams, J. T. Freymueller, T. H. Dixon, and W. G. Melbourne, " The Spring 1985 High Precision Baseline Test of the JPL GPS-Based Geodetic System: A Final Report," to be published as a JPL publication, 1987.

[11] R. I. Abbot, Y. Bock, C. C. Counselman III, R. W. King, S. A. Gourevitch, and B. J. Rosen, "Interferometric Determination of GPS Satellite Orbits," in *Proceedings of the First International Symposium on Precise Positioning with the GPS*, pp. 63–72, 1985.

[12] G. Beutler, W. Gurtner, I. Bauersima, and R. Langley, "Modeling and Estimating the Orbits of GPS Satellites," in *Proceedings of the First International Symposium on Precise Positioning with the GPS*, pp. 99–111, 1985.

[13] G. Beutler, W. Gurtner, M. Rothacher, and I. B. Schildknecht, "Evaluation of the March 1985 High Precision Baseline (HPBL) Test: Fiducial Point Concept versus Free Network Solutions," *EOS Transactions, American Geophysical Union*, vol. 67, p. 911, Nov. 4, 1986.

[14] W. W. Porter, "Solar Force-Torque Model for the GPS Space Vehicle System," Rockwell International Space Division, Downey, California, February 18, 1976.

[15] S. S. Russel and J. H. Schaibly, "Control Segment and User Performance," *Navigation*, vol. 25, pp. 74–80, 1978.

[16] E. R. Swift, "NSWC's GPS Orbit/Clock Determination System," in *Proceedings of the First International Symposium on Precise Positioning with the GPS*, pp. 51–62, 1985.

[17] H. F. Fliegel, W. A. Feess, W. C. Layton, and N. W. Rhodus, "The GPS Radiation Force Model," in *Proceedings of the First International Symposium on Precise Positioning with the GPS*, pp. 113–119, 1985.

[18] Y. Bock, S. A. Gourevitch, C. C. Counselman III, R. W. King, and R. I. Abbot, "Interferometric Analysis of GPS Phase Observations," *Manuscripta Geodaetica*, vol. 11, pp. 282–288, 1986.

[19] G. Lanyi, "Troposphere Calibration in Radio Interferometry," in *Proceedings of the International Symposium on Space Techniques for Geodynamics*, p. 184, 1984.

[20] S. E. Robinson, "A New Algorithm for Microwave Delay Estimation from Water Vapor Radiometer Data," *TDA Progress Report 42-87*, vol. July–September 1986, Jet Propulsion Laboratory, Pasadena, California, pp. 149–157, November 15, 1986.

[21] C. C. Chao, *A New Method to Predict Wet Zenith Range Correction from Surface Measurements*, JPL Technical Report 32-1526, Jet Propulsion Laboratory, Pasadena, California, 1973.

[22] G. J. Bierman, *Factorization Methods for Discrete Sequential Estimation*, New York: Academic Press, 1977.

[23] L. D. Hothem, T. Vincenty, and R. E. Moose, "Relationship Between Doppler and Other Advanced Geodetic System Measurements Based on Global Data," in *Proceedings of the Third International Geodetic Symposium on Satellite Doppler Positioning*, vol. 1, pp. 109–128, 1982.

[24] R. N. Treuhaft and G. E. Lanyi, "The Effect of the Dynamic Wet Troposphere on Radio Interferometric Measurements," *Radio Science*, vol. 22, pp. 251–265, 1987.

[25] W. I. Bertiger, S. C. Wu, J. S. Border, S. M. Lichten, B. G. Williams, and J. T. Wu, "High Precision GPS Orbit Determination Using March 1985 Demonstration Data," AIAA Paper 86-0089, AIAA 24th Aerospace Sciences Meeting, Reno, Nevada, January 6–9, 1986.

[26] A. E. Evans, "Comparison of GPS Pseudorange and Biased Doppler Range Measurements to Demonstrate Signal Multipath Effects," in *Proceedings of the Fourth International Geodetic Symposium on Satellite Positioning*, pp. 573–587, 1986.

[27] R. E. Neilan, "An Experimental Investigation of the Effects of GPS Satellite Multipath," master's thesis, University of Wisconsin, Madison, Wisconsin, 1986.

[28] Y. Bock, C. C. Counselman III, S. A. Gourevitch, and R. W. King, "Establishment of Three-dimensional Control by Interferometry with the Global Positioning System," *Journal of Geophysical Research*, vol. 90, pp. 7689–7703, 1985.

[29] P. L. Bender and D. R. Larden, "GPS Carrier Phase Ambiguity Resolution Over Long Baselines," in *Proceedings of the First International Symposium on Precise Positioning with the GPS*, pp. 357–361, 1985.

[30] M. A. Spieth, T. M. Eubanks, and J. A. Steppe, "Intercomparison of UT1 Measurements During the MERIT Campaign Period," in *Proceedings of the International Conference on Earth Rotation and the Terrestrial Reference Frame, Part II*, vol. 2, pp. 609–621, 1985.

[31] J. A. Steppe, T. M. Eubanks, and M. A. Spieth, "Intercomparison of Polar Motion Measurements During the MERIT Period," in *Proceedings of the International Conference on Earth Rotation and the Terrestrial Reference Frame, Part II*, vol. 2, pp. 622–636, 1985.

Table 1. Receiver deployment

Location	Receiver	WVR
Austin, Texas	TI-4100	–
Dahlgren, Virginia	TI-4100	–
Fort Davis, Texas	TI-4100 AFGL	–
Hat Creek, California	TI-4100	Yes
Haystack, Massachusetts	TI-4100 AFGL	–
Mammoth Lakes, California	TI-4100	–
Mojave, California	TI-4100 JPL SERIES-X	Yes
Owens Valley, California	TI-4100 JPL SERIES-X	Yes
Point Mugu, California	TI-4100	–
Richmond, Florida	TI-4100 AFGL	–

Table 2. Parameter estimation strategy

Parameter	A priori σ
Satellite positions	(20, 20, 20) km
Satellite velocities	(2, 2, 2) m/s
Non-fiducial station locations	(1, 1, 1) km
White noise clocks	0.1 sec
Polynomial clocks	0.1 sec bias 10^{-7} sec/sec rate 10^{-13} sec/sec^2 accel
Carrier phase bias	10 sec
Zenith wet tropospheric delay	20 cm (no WVR) 3 cm (WVR)
Solar radiation pressure	
X, Z, Y-bias coefficients	25%, 25%, 100%
Data weights: 1–2 cm	(white noise clocks all arcs)
2 cm	(polynomial clocks 1-day arc)
Data interval: 1 carrier ϕ meas/360 sec	

Table 3. Stochastic troposphere estimation strategies

Strategy	Process noise level	τ	σ_p a priori
1. Random walk	10 cm except Fort Davis/OVRO 3 cm Fort Davis/OVRO	∞	20 cm (SM) 3 cm (WVR)
2. Random walk	10 cm except Fort Davis 3 cm Fort Davis	∞	20 cm (SM) 3 cm (WVR)
3. Random walk	10 cm except Fort Davis 3 cm Fort Davis	∞	20 cm
4. Random walk	10 cm	∞	20 cm (SM) 3 cm (WVR)
5. Colored noise	σ_{ss} = 5 cm	12 hrs (SM) 24 hrs (WVR)	20 cm
6. Colored noise	σ_{ss} = 5 cm	12 hrs	20 cm
7. Colored noise	σ_{ss} = 10 cm	96 hrs	20 cm
8. Random walk	7.5 cm	∞	20 cm

ρ: zenith tropospheric delay
σ_ρ: uncertainty in ρ
σ_{ss}: steady state colored noise sigma Eq. (5)
Process noise level:
For random walks: cumulative effect of process noise [q_{dis} in Eq. (6)] on σ_ρ over 24 hrs
For colored noise: σ_{ss}
τ: colored noise exponential correlation time constant
WVR: ρ calibrated with water vapor radiometer measurements
SM: ρ calibrated with surface meteorology measurements

Process noise models listed in order of performance based on baseline/orbit repeatability.
Models 1–4 performed significantly better than models 5–8 or models with constant ρ.

Table 4. Consider analysis assumptions

Consider parameter	Consider σ
Fiducial coordinates	(4, 4, 4) cm
UT1–UTC	0.2 msec
X-pole	2 masec
Y-pole	2 masec
Geocenter coordinates	(10, 10, 10) cm

Five ground stations, six-day tracking arc
Fiducials: Owens Valley, Richmond, Haystack
Station and satellite clock model: white noise
Troposphere model: random walk
Carrier ϕ data interval: 1 meas/360 sec
Data weight: 1.5 cm

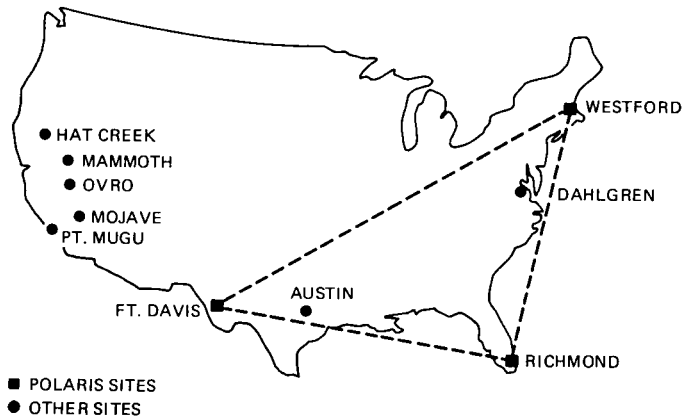

Fig. 1. Locations of GPS receivers during the spring 1985 GPS experiment

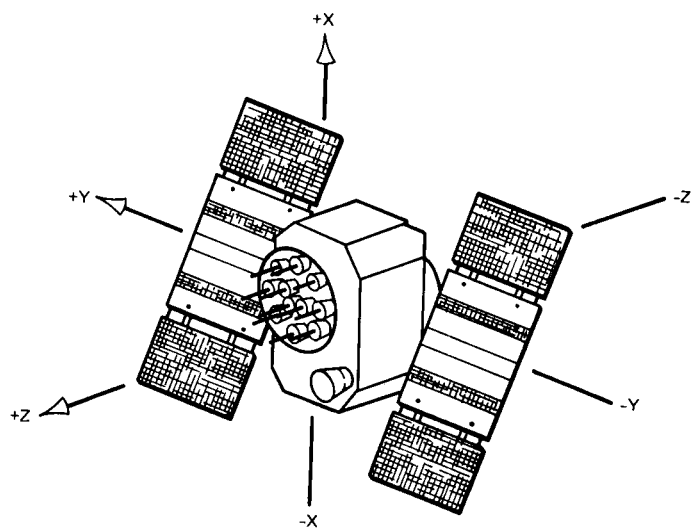

Fig. 2. Local coordinate system used to define GPS solar pressure coefficients in the ROCK4 model

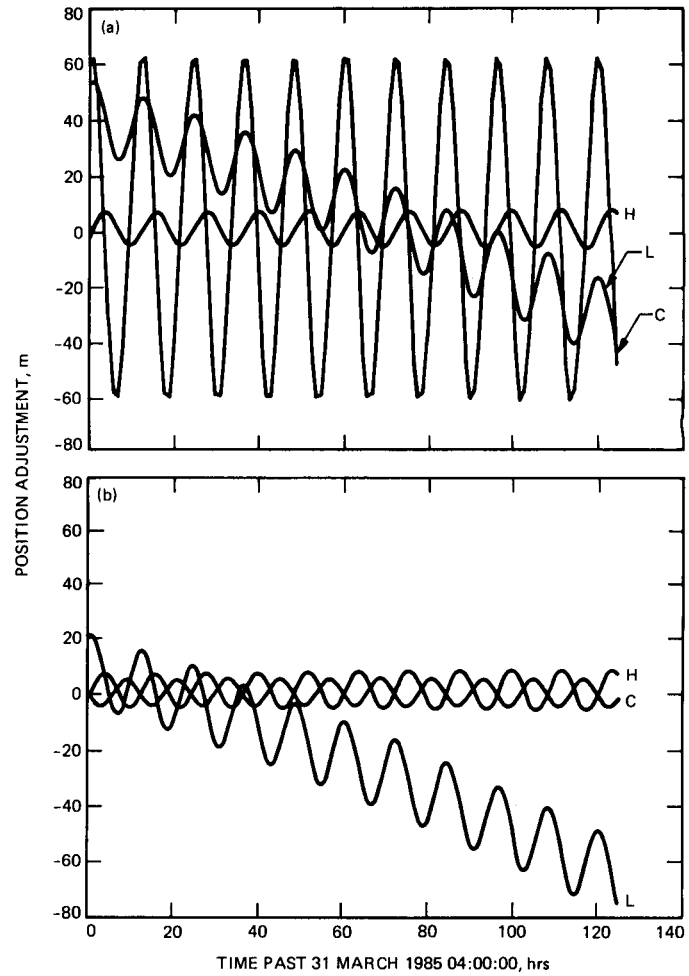

Fig. 3. Altitude (H), cross-track (C), and down-track (L) orbit adjustments for GPS 8 from a six-day arc: (a) with large orbit corrections, mostly due to coordinate system offset; (b) with ~ 3 μrad coordinate system rotation removed before orbit determination

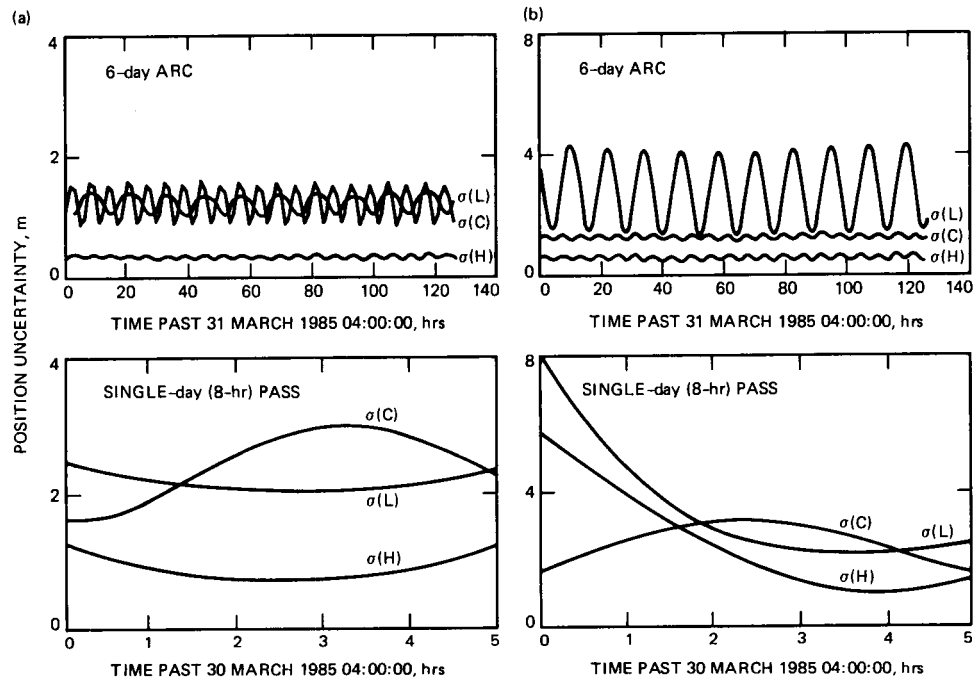

Fig. 4. Formal orbit uncertainties for satellites tracked from a six-day arc with five ground stations and from a single-day (eight-hour) pass with nine ground stations: (a) a well-tracked satellite (GPS 8); (b) a sparsely tracked satellite (GPS 6)

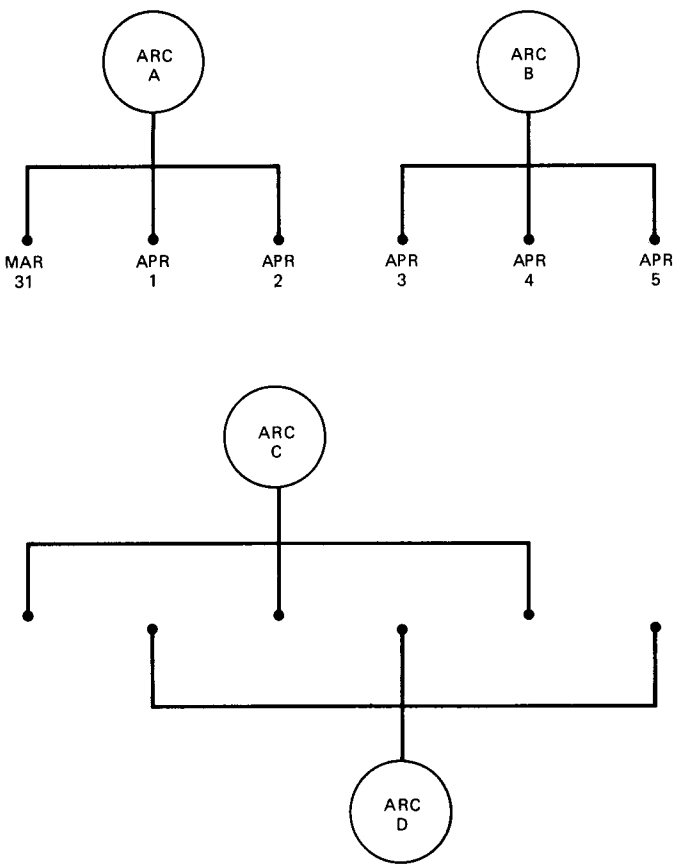

Fig. 5. Arcs A, B, C, and D used for orbit repeatability studies

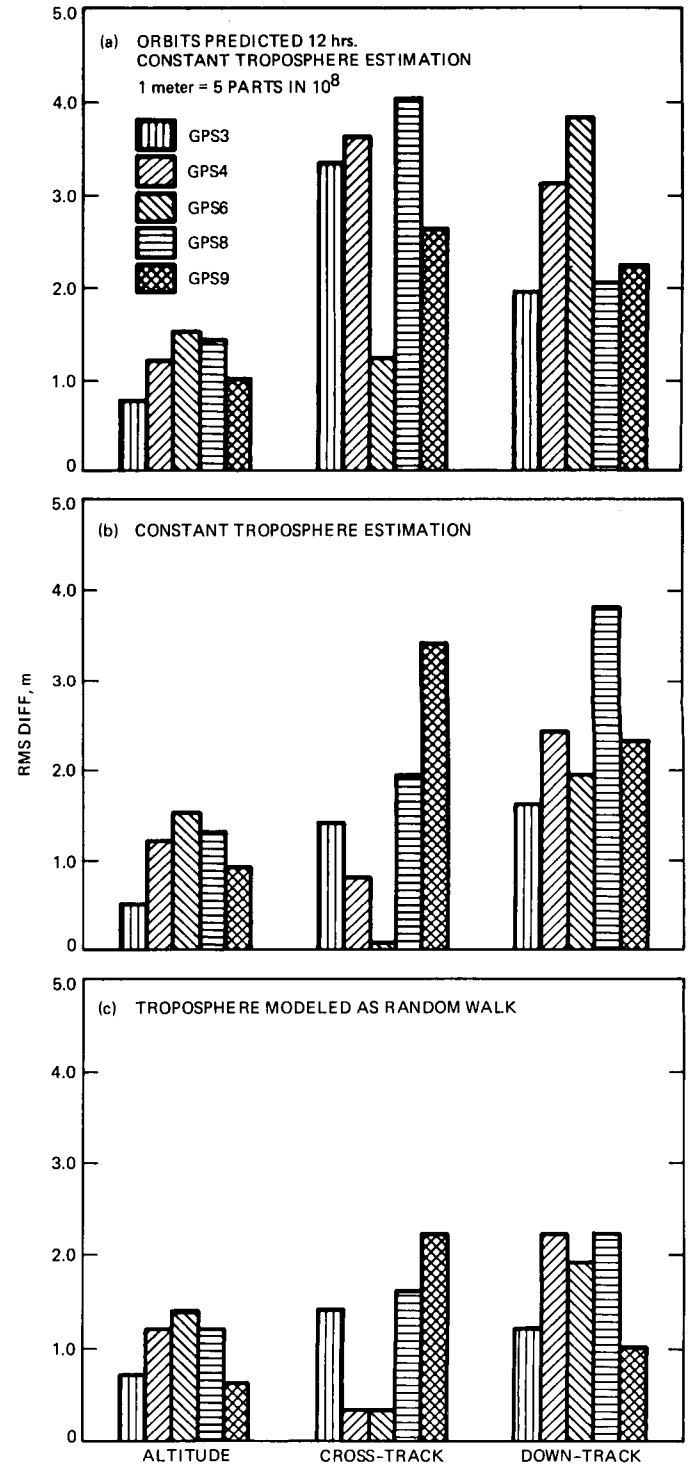

Fig. 6. Orbit repeatability for five satellites: (a) using arcs A and B with constant zenith wet tropospheric delays estimated at each station; (b) using arcs C and D with constant zenith wet tropospheric delays estimated at each station; and (c) using arcs C and D with random walk process noise models for the zenith wet tropospheric delays estimated at each station

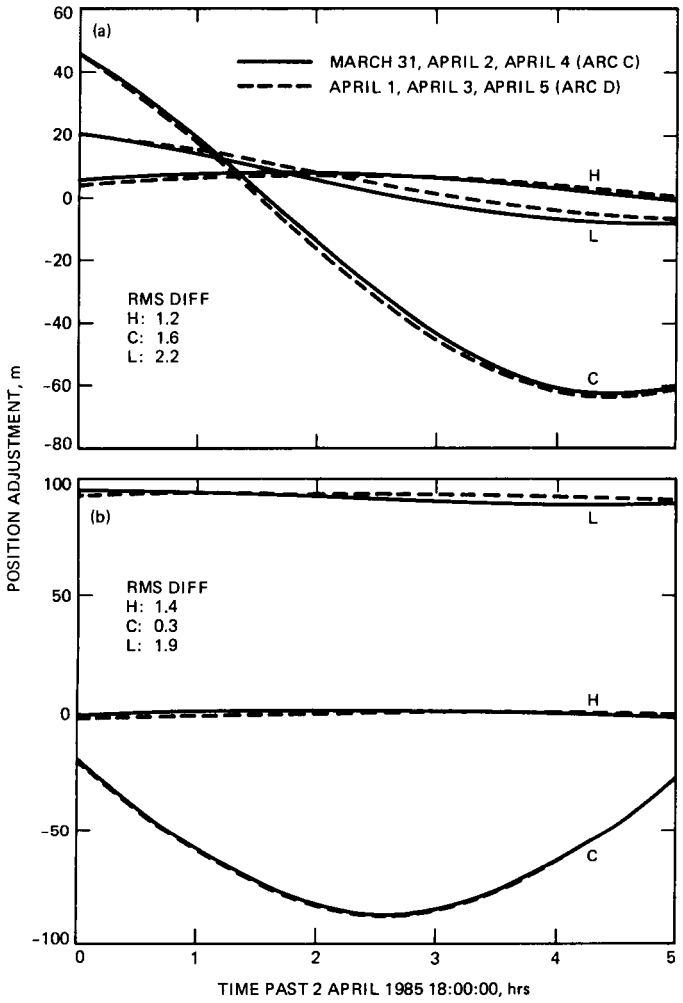

Fig. 7. Comparison of orbit solutions for (a) GPS 8 and (b) GPS 6 mapped to a six-hour period during which no observations were taken; these solutions correspond to results plotted in Fig. 6(c)

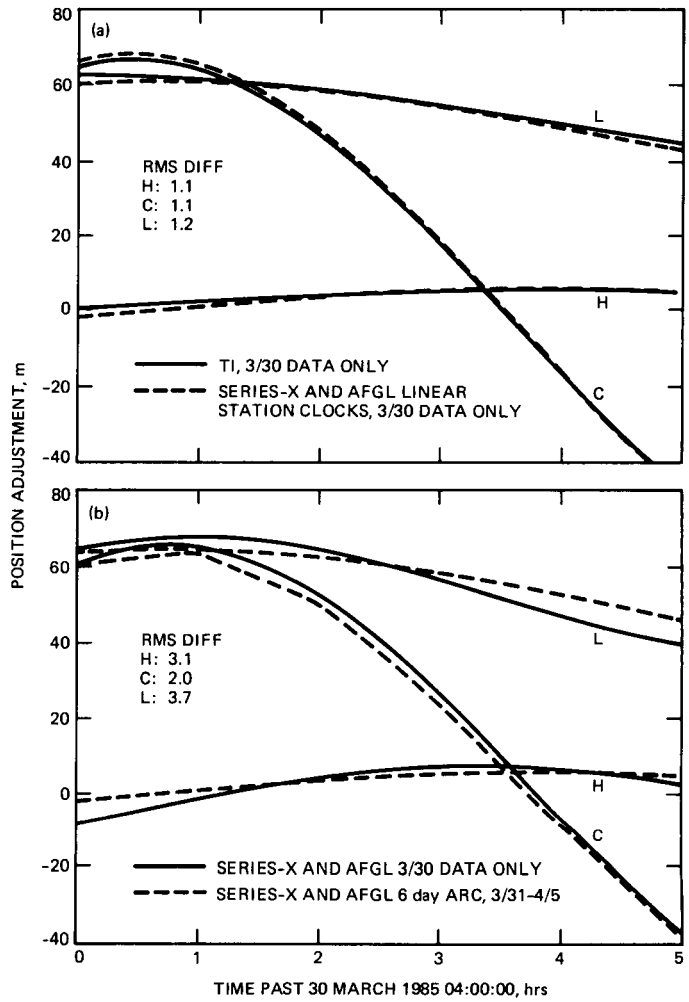

Fig. 8. Orbit repeatability for GPS 8 with (a) two single-day arcs and (b) a single-day arc and multi-day arc solutions

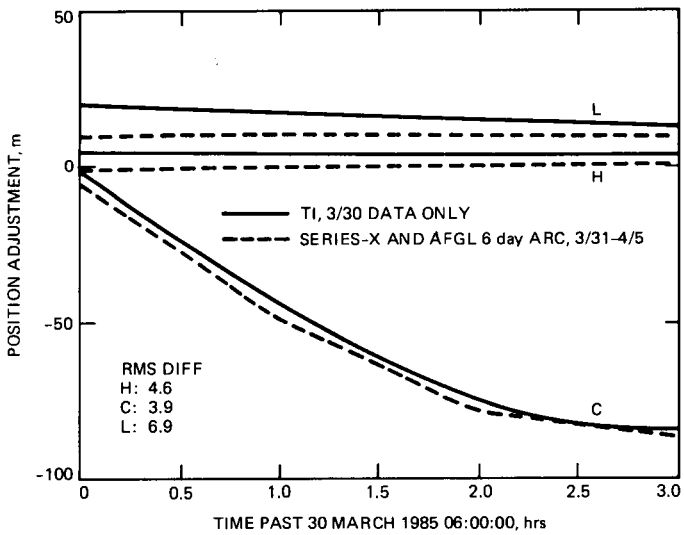

Fig. 9. Comparison of single-day and multi-day orbit solutions for GPS 6

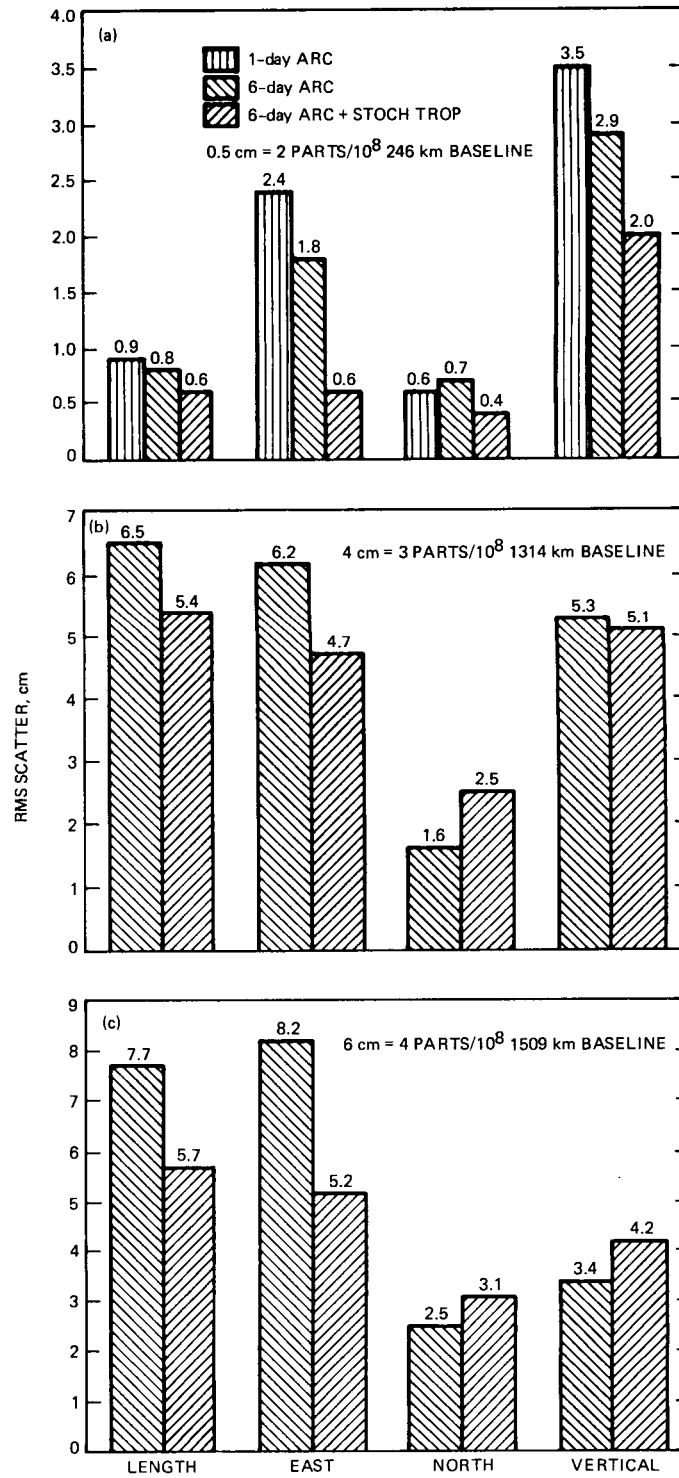

Fig. 10. Baseline repeatability for (a) Mojave-OVRO; (b) Mojave-Fort Davis; and (c) OVRO-Fort Davis

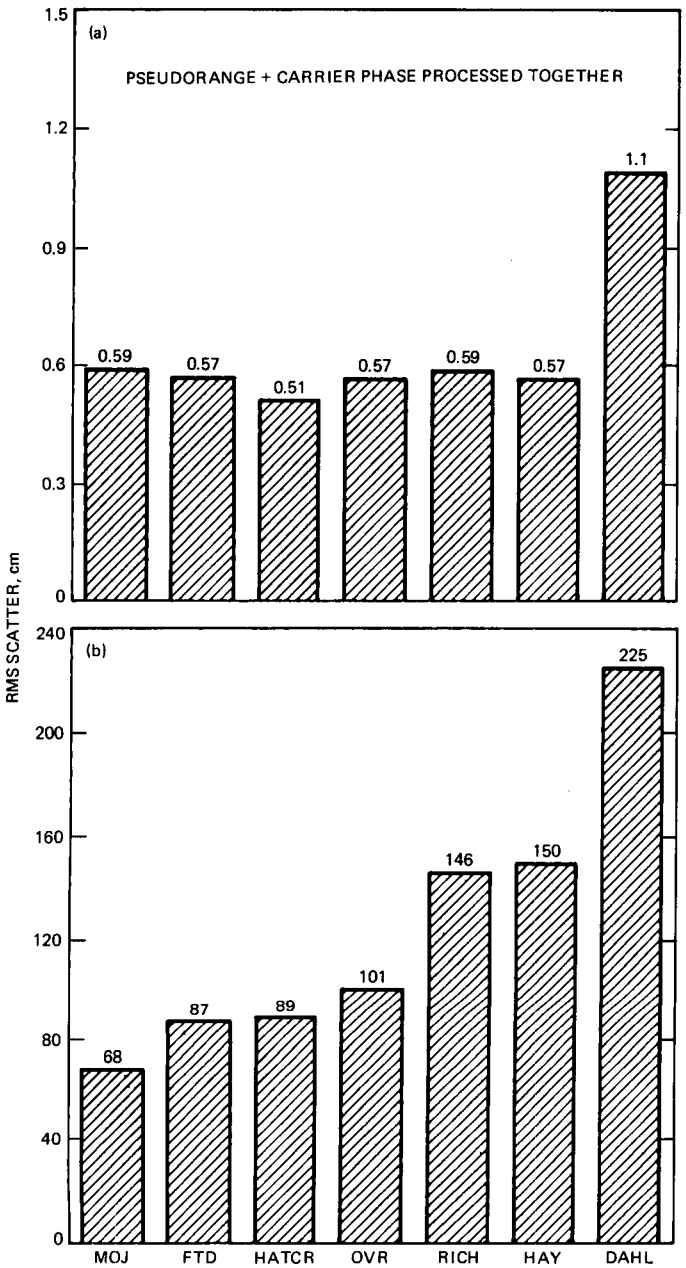

Fig. 11. Post-fit rms scatter for (a) carrier phase and (b) pseudorange from a solution in which both data types were processed together; post-fit scatter is shown for seven TI-4100 receivers

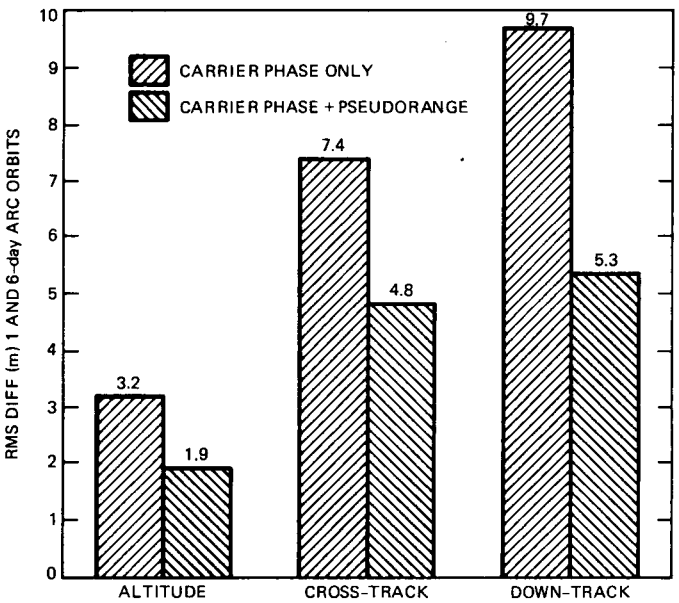

Fig. 12. Improvement in orbit repeatability resulting from processing pseudorange data together with the integrated doppler from carrier phase for a single-day pass; the single-day pass solutions are compared with a six-day, carrier-phase-only solution

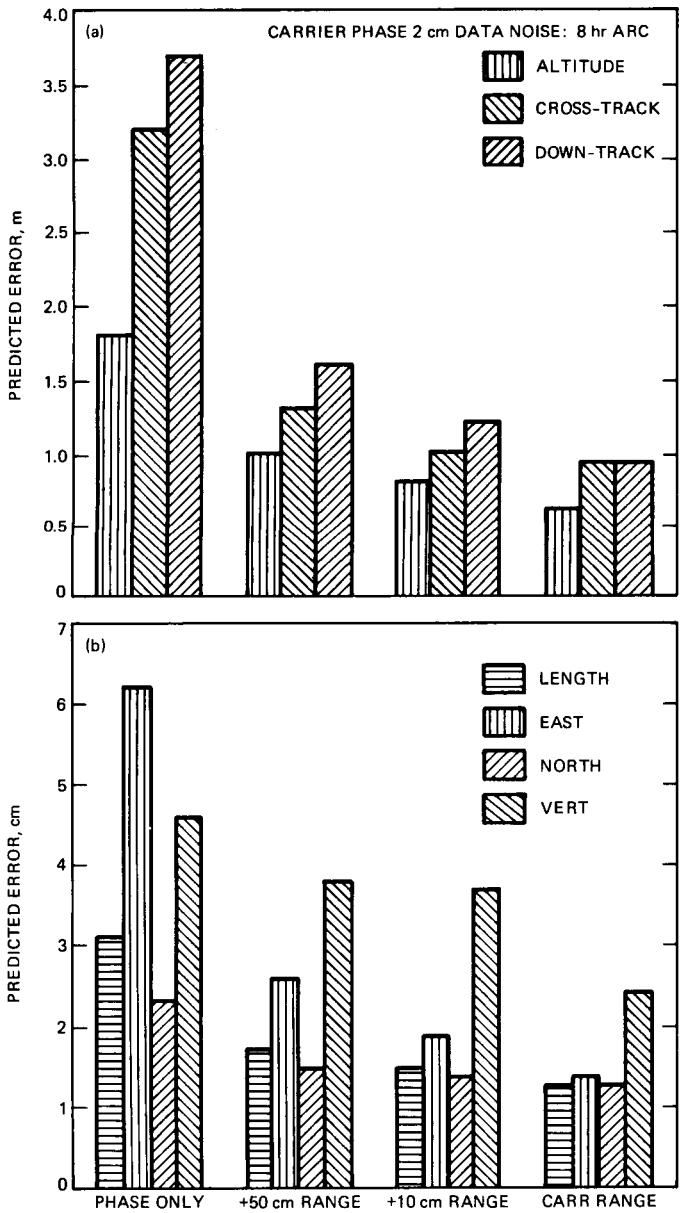

Fig. 13. Predicted reduction of orbit and baseline errors from covariance analysis when carrier phase and pseudorange data are processed simultaneously, assuming 4 cm uncertainty in fiducial station coordinates: (a) predicted orbit accuracy; (b) predicted baseline determination accuracy

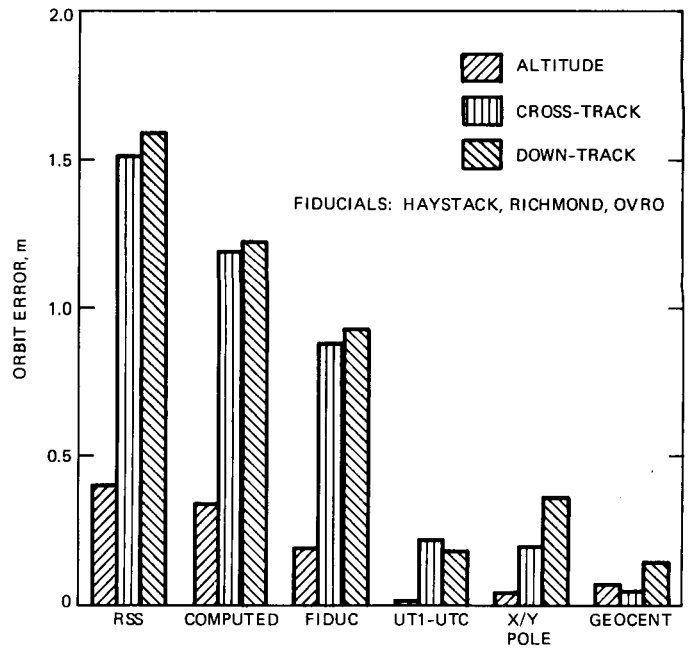

Fig. 14. Consider error analysis for carrier phase (GPS 8) showing relative contributions to the GPS error budget from data noise (computed error), fiducial station coordinate errors, earth orientation uncertainty, and geocenter location error; the configuration of the spring 1985 GPS experiment was used for this analysis